# Isolation of the Ozone QBO in SAGE II Data by Singular-Value Decomposition

WILLIAM J. RANDEL AND FEI WU

*National Center for Atmospheric Research,* Boulder, Colorado*

(Manuscript received 16 August 1995, in final form 27 March 1996)

ABSTRACT

Detailed structure of the global quasi-biennial oscillation (QBO) in ozone is analyzed using Stratospheric Aerosol and Gas Experiment II ozone and nitrogen dioxide data. Emphasis is placed on the midlatitude QBO, in particular its vertical structure and seasonal synchronization. The global QBO signal is isolated using a combination of singular-value decomposition and regression analyses, which combine to act as an accurate QBO digital filter. Results show that the midlatitude ozone QBO has a two-cell structure in the vertical (similar to that at the equator), with in-phase maxima in the lower and middle stratosphere. Both upper- and lower-level anomalies contribute important fractions to the midlatitude column amounts. The lower-level maxima have a broad latitudinal structure (~15°–60°), and collocation with the strongest background gradients suggests that these anomalies result from mean vertical transport. The middle stratosphere signal maximizes in the subtropics (10°–40°) and is likely due to nitrogen-related chemical effects (which are in turn due to transport variations). The vertically in-phase seasonal synchronization in midlatitudes is evidence of QBO modulation of the winter hemisphere circulation.

## 1. Introduction

Interannual variability in equatorial ozone is dominated by an approximate 2-yr cycle, which is closely linked with the quasi-biennial oscillation (QBO) in zonal wind and temperature in the tropical lower stratosphere. A strong QBO component in ozone is also observed in extratropics of both hemispheres. Analyses of long time series of global satellite data from the Total Ozone Mapping Spectrometer (TOMS) have clearly documented characteristics of the global QBO in column ozone (Bowman 1989; Lait et al. 1989; Chandra and Stolarski 1991; Randel and Cobb 1994; Tung and Yang 1994a; Yang and Tung 1994). The main results of these analyses show: 1) column ozone variations near the equator (±10° latitude), approximately in-phase with the equatorial zonal winds near 30 mb, and 2) extratropical anomalies over approximately 15°–60° latitude in each hemisphere, approximately out of phase with the tropical signal. The amplitude of the column ozone QBO anomalies is of order 2%–4% background values. An intriguing and as yet poorly understood aspect of the extratropical ozone QBO is that it is seasonally synchronized, such that the QBO influence is observed only during winter–spring of each respective hemisphere. Similar results have been derived from ground-based measurements (e.g., Hamilton 1989; Yang and Tung 1994) and from other satellite-derived column ozone data (Hasebe 1983; Hollandsworth et al. 1995b). Nearly identical global QBO patterns are also observed in lower-stratospheric temperature data (Randel and Cobb 1994).

The vertical structure of the ozone QBO has been analyzed using Stratospheric Aerosol and Gas Experiment (SAGE II) ozone profile data by Zawodny and McCormick (1991) and Hasebe (1994). Their results focused on the equatorial QBO, showing significant anomalies in the lower stratosphere (20–27 km) and in the middle stratosphere (30–38 km), with a node near 28 km. These studies furthermore noted significant QBO modulations in tropical nitrogen dioxide ($NO_2$), and Chipperfield et al. (1994) demonstrated from model results that the two-cell structure in ozone was due to mean vertical transport (in the lower stratosphere) and reactive nitrogen ($NO_y$) associated chemical effects (in the middle stratosphere), respectively.

The work here presents a further analysis of the SAGE II data, with focus on studying the extratropical ozone QBO, in particular its detailed vertical structure and seasonal synchronization. The analyses here are based on singular-value decomposition (SVD) and regression analyses of SAGE II constituent data together with the QBO zonal winds; these analyses allow accurate isolation of the global QBO signals. Our results

* The National Center for Atmospheric Research is sponsored by the National Science Foundation.

*Corresponding author address:* Dr. William J. Randel, Atmospheric Chemistry Division, National Center for Atmospheric Research, P.O. Box 3000, Boulder, CO 80307-3000.

demonstrate the importance of both middle- and lower-stratospheric contributions to midlatitude ozone QBO anomalies and show that both chemical and dynamic processes must be included in a proper global QBO simulation.

## 2. Data and analyses

The primary datasets analyzed here are ozone and nitrogen dioxide ($NO_2$) mixing ratios from SAGE II. These data are reviewed and discussed in McCormick et al. (1989) and Zawodny and McCormick (1991). SAGE II uses a solar occultation measurement technique, obtaining 15 sunrise and 15 sunset measurements per day, each near the same latitude, but spaced ~24° apart in longitude. The latitudinal sampling progresses in time, so that much of the latitude range 55°N–55°S is sampled in one month. The vertical resolution of these data is 1 km, and zonal averages are binned into monthly samples on a 4° latitude grid prior to further analyses. The time period spans November 1984–May 1991 (data after the Mt. Pinatubo eruption are omitted). We combine sunrise and sunset ozone data, and examine the altitude range 18.5–50.5 km. Because of the strong diurnal variation of $NO_2$ we examine only sunset measurements, with data spanning 18.5–45.5 km. As discussed by Zawodny and McCormick (1991), Gray and Chipperfield (1990), and Chipperfield et al. (1994), the QBO signal in sunset $NO_2$ measurements is primarily due to QBO-modulated transport of total reactive nitrogen ($NO_y$).

For longer term perspective of the QBO and comparison of SAGE II profiles with column ozone data, we also use column ozone (measured in Dobson units where 1 DU = $2.142 \times 10^{-5}$ kg m$^{-2}$) derived from solar backscatter ultraviolet (SBUV) measurements on *Nimbus 7,* combined with SBUV/2 data from *NOAA-11,* spanning November 1978–October 1994. Column ozone measurements derived from SBUV/2 are not strongly degraded by the Pinatubo aerosols (Bhartia et al. 1994). Details of merging these datasets and an atlas of global ozone variability based on this long record are available in Randel and Wu (1995).

The statistical analysis we use to isolate the global ozone QBO is based in part on singular-value decomposition (SVD). SVD involves a matrix operation applied to covariances between gridpoint observations of two fields. It determines optimal modes of covariability between the two fields and is conceptually similar to empirical orthogonal function (EOF) analyses of one field of data [the work here is an extension of the QBO EOF analyses of Wallace et al. (1993)]. A detailed discussion of SVD and its application to idealized and observed data may be found in Bretherton et al. (1992) and Wallace et al. (1992). For the analyses here the two fields of data are the deseasonalized constituent anomalies (either ozone or nitrogen dioxide, as a function of latitude, altitude, and time) and the deseasonalized equatorial zonal winds over 70–10 mb (as function of altitude and time). SVD analyses of these fields determines constituent variations that are temporally coherent with the QBO winds; output of the analyses are sets of coupled constituent zonal wind modes (spatial structures), along with eigenvalues quantifying the percentage covariance explained by the respective modes. Time variation is determined by projection of the spatial structures onto the original anomalies.

One further consideration in the SVD analysis is the choice of using mixing ratio anomalies versus local percentage variations (i.e., values divided by the long-term background zonal means). This choice can make a difference in the detailed structure of the SVD modes for constituents whose background fields vary strongly with altitude; the SVD analysis will preferentially weight the regions of maximum variance. We have compared results for the different fields here and choose percentage anomalies for ozone (in order to give more equal weight to lower stratospheric variations) and mixing ratio anomalies for nitrogen dioxide (to highlight middle stratospheric variations). Note that these choices have no effect on the regression analyses or the net isolation of the QBO signal shown below.

## 3. Results

### *a. Background—Global column ozone anomalies*

As background for the SAGE II results below, we first consider the observed global ozone anomalies associated with the QBO. Figure 1a shows a latitude–time diagram of column ozone anomalies from combined SBUV + SBUV/2 data spanning 1979–1994 (Hollandsworth et al. 1995a; Randel and Wu 1995). Anomalies here are defined as deviations from a seasonally varying background (calculated from the entire record), and additionally a linear trend over 1979–1994 has been removed (i.e., the trend shown in Hollandsworth et al. 1995a); no other signals have been removed here. Additionally, the anomalies in Fig. 1 have been multiplied by cos(latitude) to represent area weighting. The tropical ozone anomalies in Fig. 1a clearly exhibit a QBO variation, and this is furthermore demonstrated in Fig. 2, which shows a time series of the SBUV + SBUV/2 equatorial ozone anomalies together with a reference QBO time series based on the equatorial stratospheric zonal winds. Figure 1b shows the near-global QBO column ozone variation derived by seasonally varying regression analyses of the data in Fig. 1a onto the QBO reference time series shown in Fig. 2. [This reference time series is calculated from a linear combination of the equatorial zonal winds over 70–10 mb, with the following weights: 10 mb (0.24), 15 mb (0.51), 20 mb (0.60), 30 mb (0.50), 40 mb

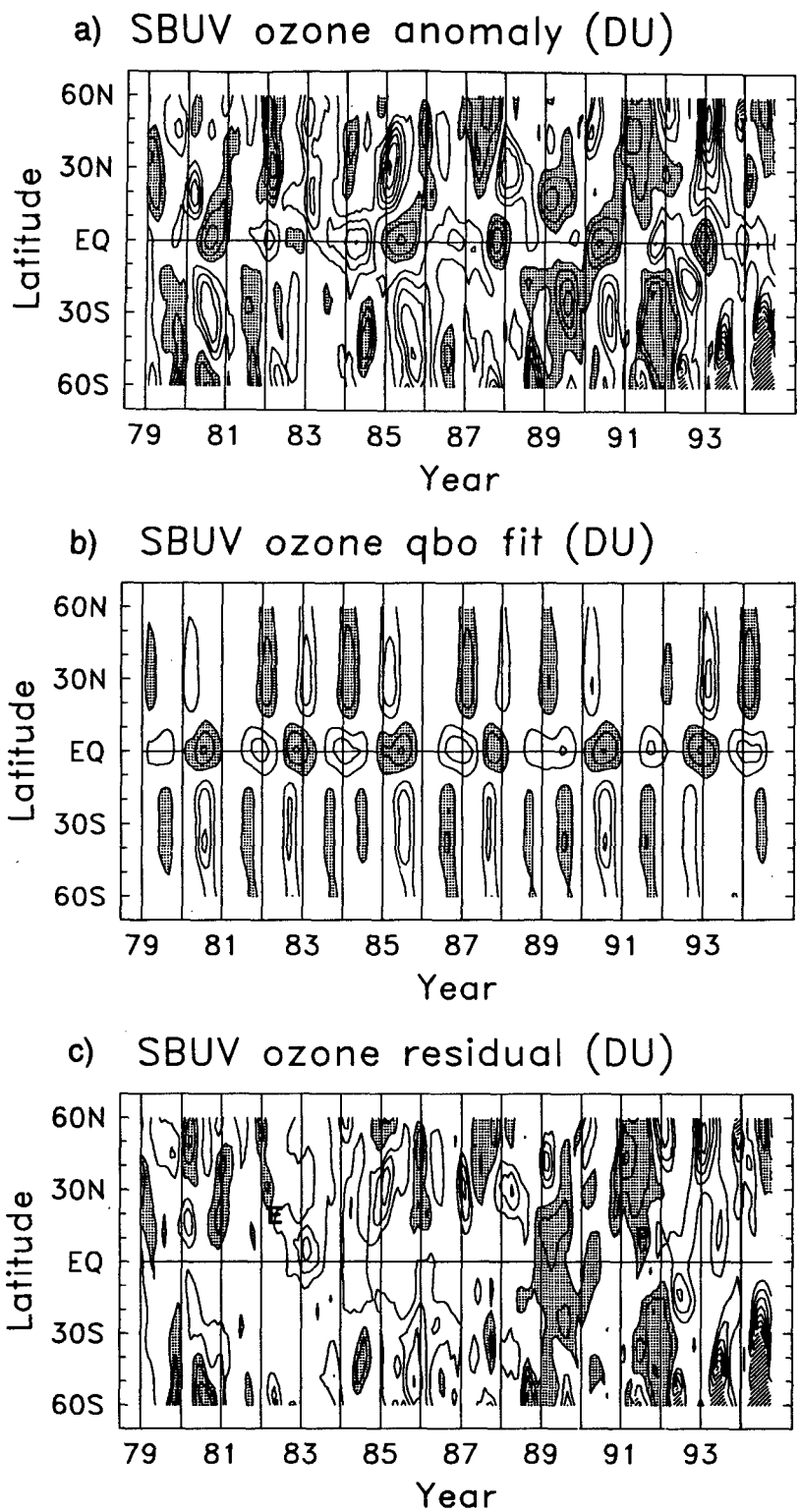


FIG. 1. Latitude–time sections of column ozone anomalies from combined SBUV–SBUV/2 data. Shown are (a) full anomalies, defined as deseasonalized and detrended over 1979–94, (b) the QBO component, derived by seasonally varying regression analysis, and (c) residual anomalies (full minus QBO). Data in all panels have been multiplied by cos(latitude) to account for area weighting. Contour interval is 3 Dobson units (DU), with zero contours omitted and positive values shaded.

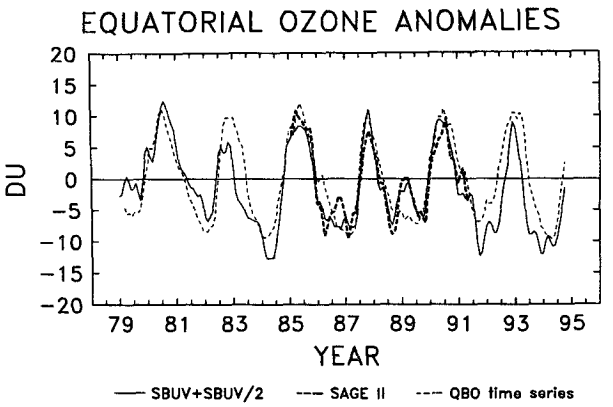


FIG. 2. Solid line shows deseasonalized column ozone anomalies over the equator from combined SBUV + SBUV/2 data. Light dashed line is a QBO reference time series, derived from a linear combination of the equatorial zonal winds over 70–10 mb, as described in text. Heavy dashed lines are column ozone anomalies from SAGE II data, derived by vertically integrating the ozone density anomalies shown in Fig. 4a.

(0.26), 50 mb (0.04), and 70 mb (−0.09). These weights were calculated empirically to optimize the fit to column ozone, neglecting volcanically perturbed periods.] The SBUV + SBUV/2 global QBO patterns in Fig. 1b are similar to those derived from TOMS data (Bowman 1989; Yang and Tung 1994), in particular showing large anomalies over 15°–60° in each hemisphere, approximately out of phase with the tropical patterns. An important aspect of these subtropical–midlatitude anomalies is that they are seasonally synchronized, with large amplitude only during winter–spring seasons in each respective hemisphere (see above references); this is why it is necessary to use seasonally varying regression to accurately fit the QBO anomalies away from the equator. Figure 1c shows the remaining column ozone anomalies after removal of the QBO. Comparison of the separate panels in Fig. 1 shows the importance of the QBO in both Tropics and midlatitudes and demonstrates that correct isolation of QBO effects is crucial for evaluating other sources of interannual variability.

Besides the QBO ozone variations in the Tropics and low–midlatitudes discussed above, analyses of TOMS data and other long-term records suggest a further region of QBO influence in the winter polar vortices (Oltmans and London 1982; Garcia and Solomon 1987; Bowman 1989; Lait et al. 1989; Randel and Cobb 1994). The polar ozone QBO is approximately in phase with midlatitudes (and out of phase with the Tropics) and also seasonally synchronized (maximum in spring). Observational evidence for the polar ozone QBO is less statistically significant than that in the Tropics or midlatitudes, at least partly because of the high level of "natural" interannual variability in vortex structure. Because the sampling of the SAGE II instrument includes polar regions for only short time periods, the polar lobe of the ozone QBO is not analyzed here.

### *b. SAGE II ozone analyses*

For isolation of interannual QBO effects, it is first necessary to accurately estimate seasonal variations. One technique that works well for the irregularly sampled SAGE II data is the fitting of annual and semi-

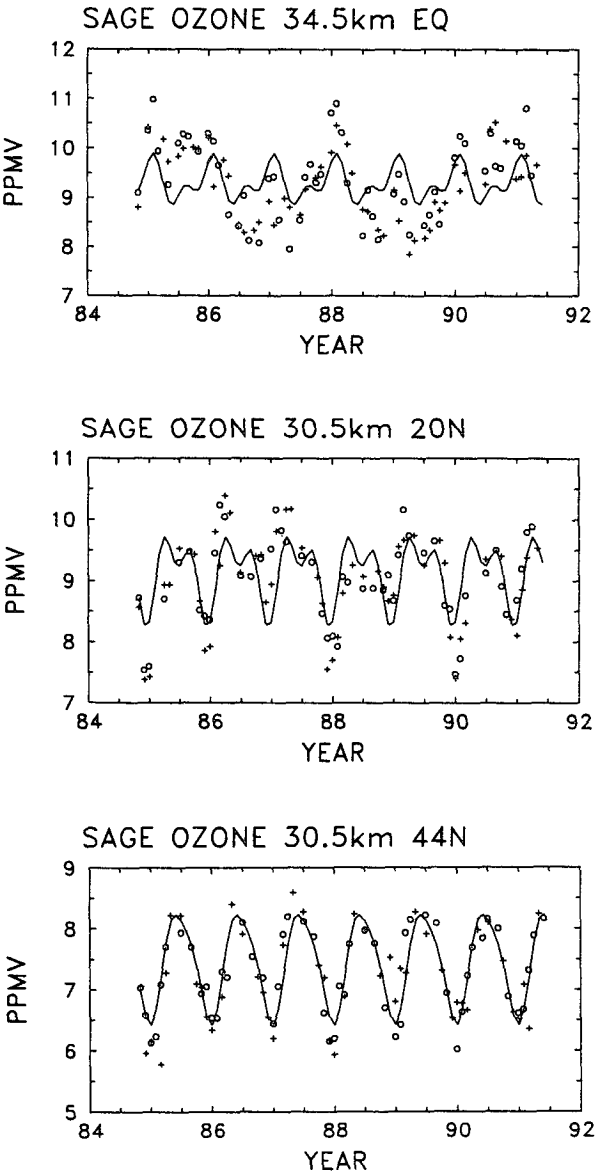


FIG. 3. Time series of sunrise (circles) and sunset (pluses) SAGE II ozone data at the indicated locations. Smooth curves show (repeating) annual cycles derived from harmonic regression fits of these data.

annual harmonics to the data at each latitude and altitude. Figure 3 shows the ozone data and fit annual cycles over the equator at 34.5 km and at 20° and 44°N at 30.5 km. The seasonal cycle is predominantly an annual harmonic at midlatitudes (44°), whereas in low latitudes there is important contribution from the semiannual harmonic [in agreement with the SBUV analyses of Perliski and London (1989) and SAGE II results of McCormick et al. (1989)]. Monthly mean interannual anomalies are defined by simply subtracting the seasonal harmonic fits, and these are the basis for all further analyses.

Figure 4a shows the resulting interannual ozone anomalies over the equator, with the results here calculated in terms of ozone density [in Dobson units DU per kilometer]. (Figure 4b shows the statistical QBO fit of these anomalies, as discussed below.) Ozone density is used in Fig. 4 in order to visually determine contributions to the column ozone anomaly (simply a sum in the vertical of the ozone density anomalies). The numerically summed column ozone amounts derived from these data are included as the heavy dashed line in Fig. 2; because these values agree well with the SBUV + SBUV/2 column ozone, this demonstrates that almost all of the equatorial column ozone variability is explained by the profile information in Fig. 4a. The QBO completely dominates the variability in Fig. 4a, with alternating positive and negative anomalies that can be traced downward in time. There are two regions of maximum ozone perturbation: in the lower stratosphere (20–27 km) and middle stratosphere (30–37 km). The anomalies at these levels are approximately one-quarter cycle out of phase, and both levels contribute significantly to column ozone variations. Similar tropical ozone QBO anomalies from SAGE II data have been shown in Zawodny and McCormick (1989), Hasebe (1994), and Chipperfield et al. (1994). Isolation of the QBO ozone signal at the equator is relatively easy because it completely dominates interannual variability. This is not the case in midlatitudes, however, where the QBO component is of similar size to other variability (e.g., Fig. 1).

As examples of the effect of the ozone QBO, Fig. 5 shows global ozone fields during the two extreme phases: April 1985 and April 1989. The QBO has a clear visual effect on the tropical ozone mixing ratio values over 30–40 km, with upward bending isolines in the positive phase (April 1985) and downward bending equatorial patterns in April 1989. The resulting double peaked (or "rabbit-ears") structure in April 1989 is similar to patterns observed in SAGE II aerosol data (Trepte and Hitchman 1992).

Results of the SVD analyses between the global ozone anomalies and the QBO zonal winds show that the first two modes (termed SVD1 and SVD2) explain 72% and 25% of the overall covariance, respectively. (Two such modes are typical for a regularly propagating oscillation, analogous to a sine and cosine Fourier decomposition for a traveling harmonic wave.) The spatial structure of these modes is shown in Fig. 6 (for ozone) and Fig. 7a (for zonal wind). SVD1 in ozone exhibits a two peak (in altitude) maximum over the equator, similar to the structure seen in Fig. 4. Additionally, there are out of phase (negative) maxima in the lower stratosphere over midlatitudes of both hemispheres and additionally over the subtropics in the middle stratosphere (i.e., the subtropics exhibits a similar two-peaked vertical structure as that seen over the equator but of the opposite sign). Ozone SVD2 is qualitatively similar to SVD1, with the patterns approximately in quadrature with SVD1 (note that these modes are orthogonal by construction). The zonal wind spatial structures (Fig. 7a) show a mode that peaks over 10–20 mb (SVD1) and over 30–40 mb (SVD2); these are

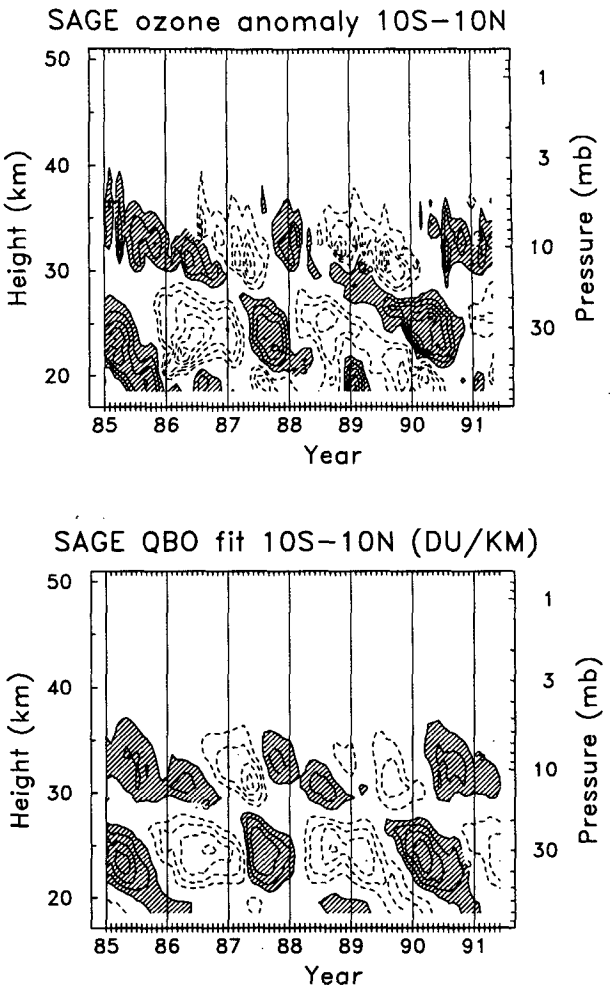


FIG. 4. Altitude–time sections of interannual ozone density anomalies over the equator. Panel (a) shows the full anomalies (departures from harmonic seasonal cycles), while (b) shows results of the statistical QBO fit. Contour interval is 0.3 DU/km, with zero contours omitted.

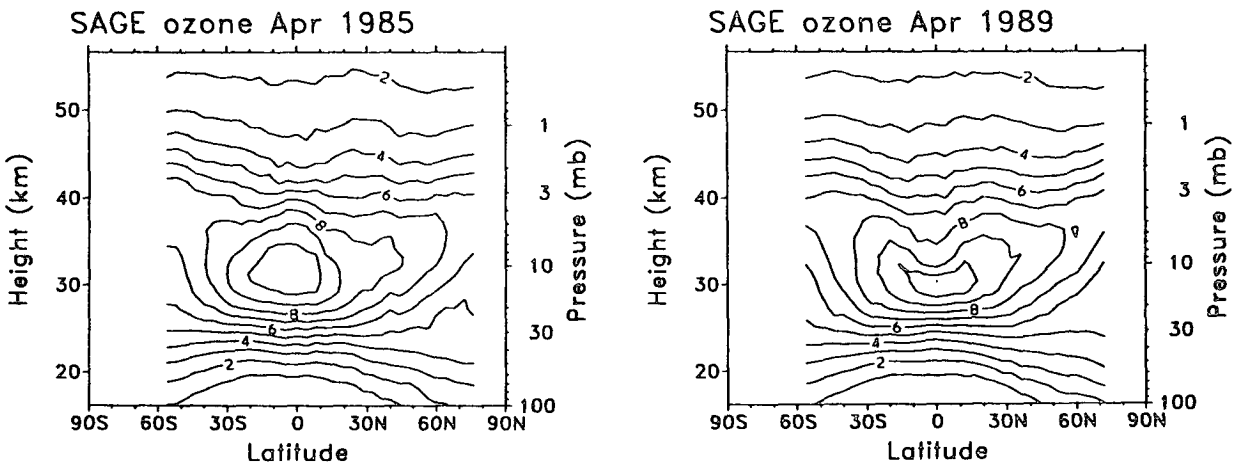


FIG. 5. Cross sections of ozone mixing ratio (ppmv) during opposing phases of the QBO in April 1985 and April 1989.

similar to the QBO wind EOF modes derived by Wallace et al. (1993). Time projection of the zonal wind SVD structures is shown in Fig. 7b; note that the projections are shown for the period 1979–1994 (for reference and comparison to Fig. 2), although the SVD spatial structures (Fig. 7a) are calculated from data over 1985–1991.

Time variation of the ozone QBO is determined by projection of the two SVD spatial structures (shown in Fig. 6) onto the global ozone anomalies. Figure 8 shows a "phase space" plot of the projections of SVD1 and SVD2 (each smoothed slightly in time); time progression corresponds to clockwise transits (or orbits of the ozone QBO), with one cycle corresponding to a QBO cycle (note there are ~2.5 cycles in this 6.5-yr record). Figure 9 shows a second method of analyzing these same data in terms of amplitude and phase of the projection points in Fig. 8. The amplitude shows substantial variations in time, with a minimum in the middle of 1988 and maxima during August–October of several years.

The amplitude of the zonal wind SVD projections is also included in Fig. 9 [a longer time series of a nearly identical quantity covering 1956–1990 is shown in Wallace et al. (1993, their Fig. 8)]. An interesting feature is that there is a minimum in the amplitude of this "dynamical" QBO index in early 1988, slightly preceding the ozone QBO minimum. This short time sample suggests that the ozone QBO may be modulated similarly to the dynamic QBO over long timescales (as described in Wallace et al. 1993).

An important aspect of the ozone QBO is its seasonal synchronization away from the equator, yet the prior

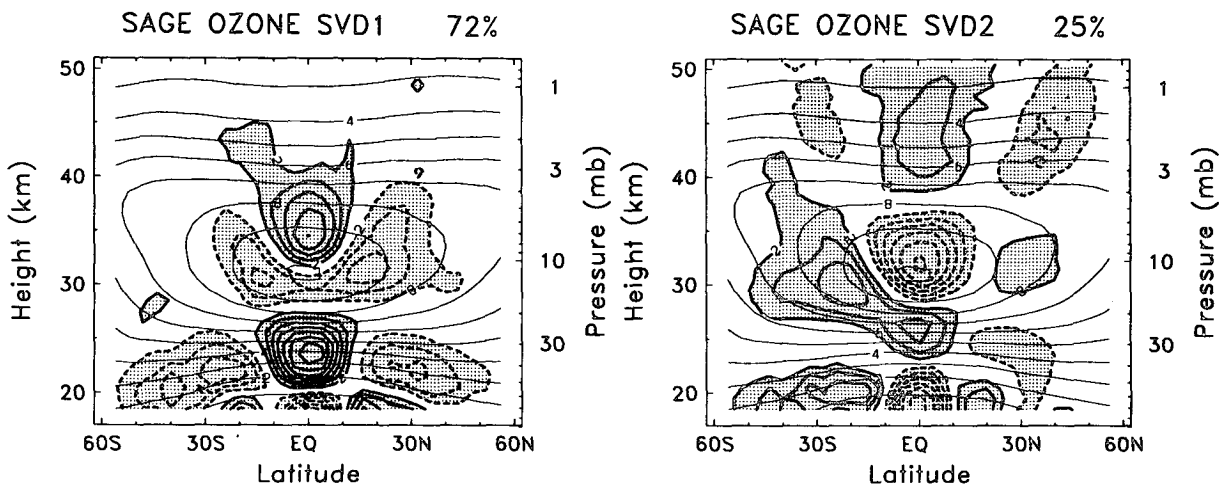


FIG. 6. Heavy solid and dashed lines with shading show spatial structure of ozone SVD1 (left) and SVD2 (right). Contour values correspond to local percent variations with arbitrary units. Light lines show background annual average zonal mean ozone.

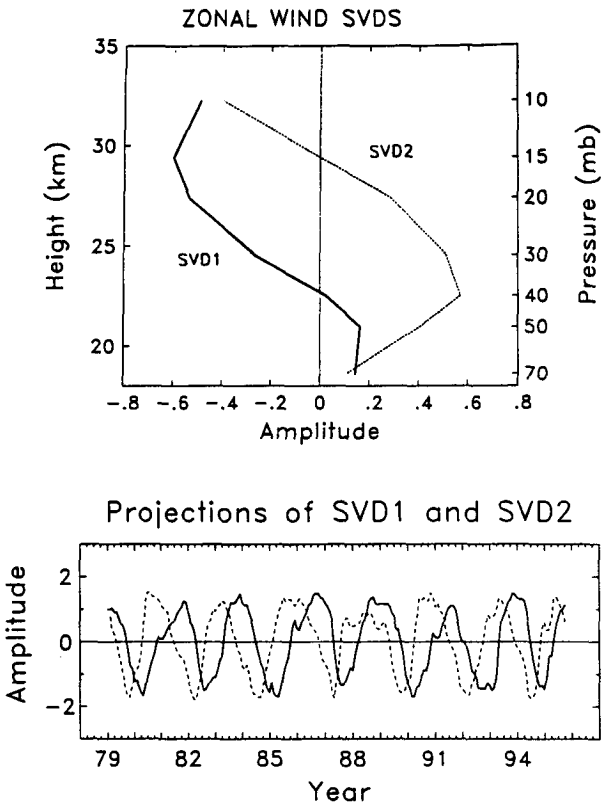


FIG. 7. Top panel shows vertical structure of zonal wind SVD1 and SVD2. Lower panel shows the time projection of these structures onto the QBO zonal wind anomalies over 1979–1994. Amplitude units in both panels are arbitrary.

SVD analyses do not allow isolation of such seasonality. In order to include seasonal variability, we isolate the ozone QBO patterns based on seasonally varying regression analysis using

$$O(t) = \alpha S1(t) + \beta S2(t). \quad (1)$$

Here S1 and S2 are time projections of the zonal wind SVD structures shown in Fig. 7b; the prior SVD analysis has determined these optimal temporal structures (and shown that two independent time series are sufficient to explain nearly all of the ozone QBO variance). Seasonality is included in Eq. (1) by defining $\alpha = A_1 + A_2 \sin\omega t + A_3 \cos\omega t$ ($\omega = 2\pi/365$ days), and likewise for $\beta$. There are thus six coefficients determined by the regression fit at each latitude and altitude.

Figure 10 shows the spatial structure of the coefficient in Eq. (1) for projections during January–March and July–September; these indicate the spatial locations of the regressed QBO anomalies during these months. For reference, the patterns are superimposed over the respective background zonal mean structures (note the seasonality in these background fields). These spatial patterns are very similar to the ozone SVD1 structure in Fig. 6 (as expected) but exhibit strong seasonal dependence in midlatitudes. In particular, the extratropical (negative) patterns are large only in the respective winter hemispheres.

Figure 11 shows examples of the QBO regression fits for the same time series shown in Fig. 3. Note the higher-frequency components of the fits away from the equator and also the fact that relatively less of the overall variance is explained by the QBO at 44° versus 20°N (in agreement with the variance partitioning seen in Fig. 1). The regression analysis here allows a smooth, continuous mapping of the QBO signal in latitude, altitude, and time; this technique may be viewed as an accurate digital filter to isolate QBO variability. Figure 4b shows the associated QBO fit of the equatorial ozone anomalies, for comparison with the "full" anomalies (in Fig. 4a). As expected, a predominance of the variability at the equator projects onto the QBO.

Figure 12 shows the interannual ozone anomalies and the statistical QBO fit at 30°S (expressed in terms of ozone density, as in Fig. 4). The QBO accounts for a large fraction of interannual variance at this latitude (as at the equator). There is a two-cell vertical structure to the anomalies, and they are vertically in phase [as opposed to variations in quadrature over the equator (Fig. 4)]. Note that the anomalies at both levels occur preferentially during SH winter. The upper-level anomalies (over 27–32 km) contribute approximately one-third of the column anomalies, versus approximately two-thirds from the lower-level maximum over 19–24 km.

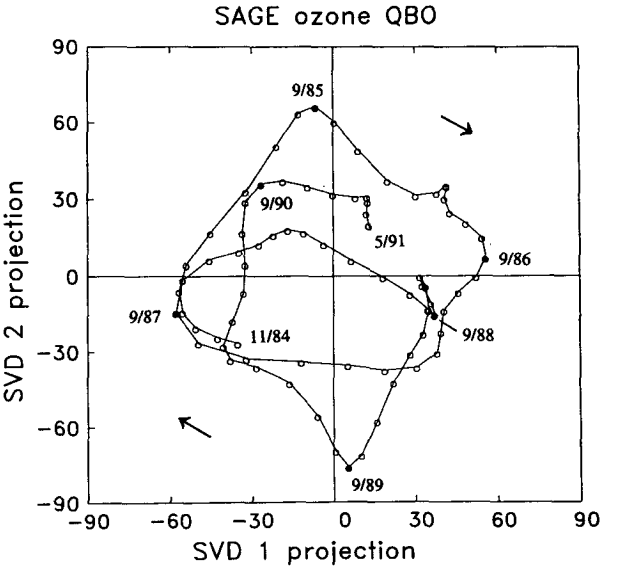


FIG. 8. Phase space diagram of the projection of the monthly global ozone anomalies onto spatial structures SVD1 and SVD2 (shown in Fig. 6). Time progression coincides with clockwise orbit transits, with locations during several individual months noted.

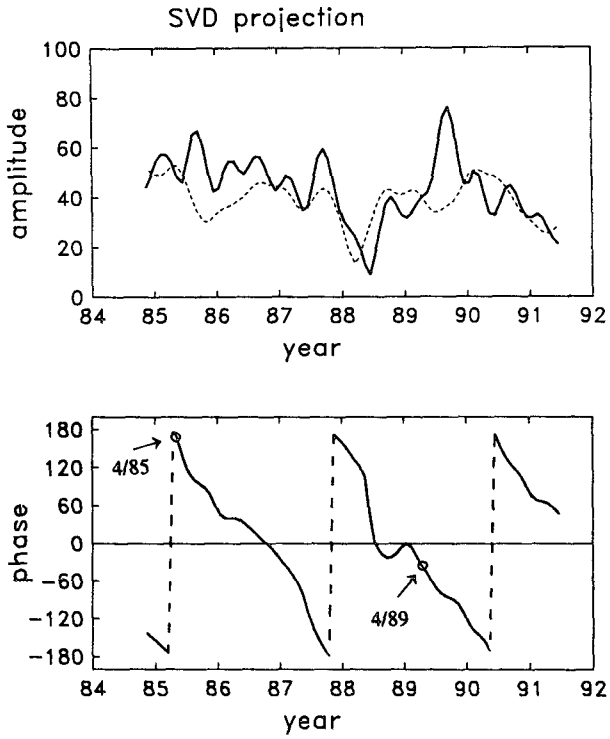


FIG. 9. Top panel shows time series of the amplitude of the projections of SVD1 and SVD2, $(SVD1^2 + SVD2^2)^{1/2}$, for ozone (solid line) and equatorial zonal wind (dashed). Units are arbitrary. Bottom panel shows phase variation of the ozone SVD projection, $=\tan^{-1}(SVD1/SVD2)$ (i.e., the phase variation of the data in Fig. 8). Circles denote April 1985 and 1989, the time samples shown in Fig. 5. Phase of the zonal wind projections is nearly identical and not shown.

Figure 13 shows the QBO ozone density variations versus latitude at 22.5 and 30.5 km. These are plotted using the same contour interval, so that the relative contribution of the upper- and lower-level anomalies to the column can be assessed. Furthermore, Fig. 14 shows the QBO column ozone variations derived by vertically integrating the SAGE II profile density data, together with the SBUV + SBUV/2 QBO fit over 1985–1991 [as in Fig. 1b, but not weighted by cos(latitude) here]. The QBO column ozone variations calculated from the SAGE II data are in good agreement with those derived from SBUV + SBUV/2 data, both in the Tropics (as shown in Fig. 2) and in midlatitudes. Comparison of the latitude–time sections in Fig. 13 and the column data in Fig. 14 illustrate the relative importance of the middle- and lower-stratosphere contributions to the midlatitude column amounts. These data show that the upper-level anomalies contribute substantially to the column, particularly in the subtropics (10°–40°). The lower-level patterns have a broad latitudinal structure (15°–60°) and are the predominant contributor to the column at high latitudes (40°–60°N–S). Note that the extratropical anomalies at both upper and lower levels in Fig. 13 are seasonally synchronized, leading to the column ozone synchronization. Time periods that exhibit relatively large midlatitude column deviations (such as in the SH in 1985, 1989, and 1990) exhibit large in-phase contributions from both upper and lower levels (see also Fig. 12). Overall both the middle- and lower-stratospheric anomalies are important components of the midlatitude ozone QBO. Because the lower-stratospheric maxima occur precisely in the region of strong background vertical gradient (see Figs. 6 and 10), they are likely attributable to mean vertical advection effects (discussed further below). Conversely, the upper-level anomalies occur near the background maximum, and thus are due to a different cause.

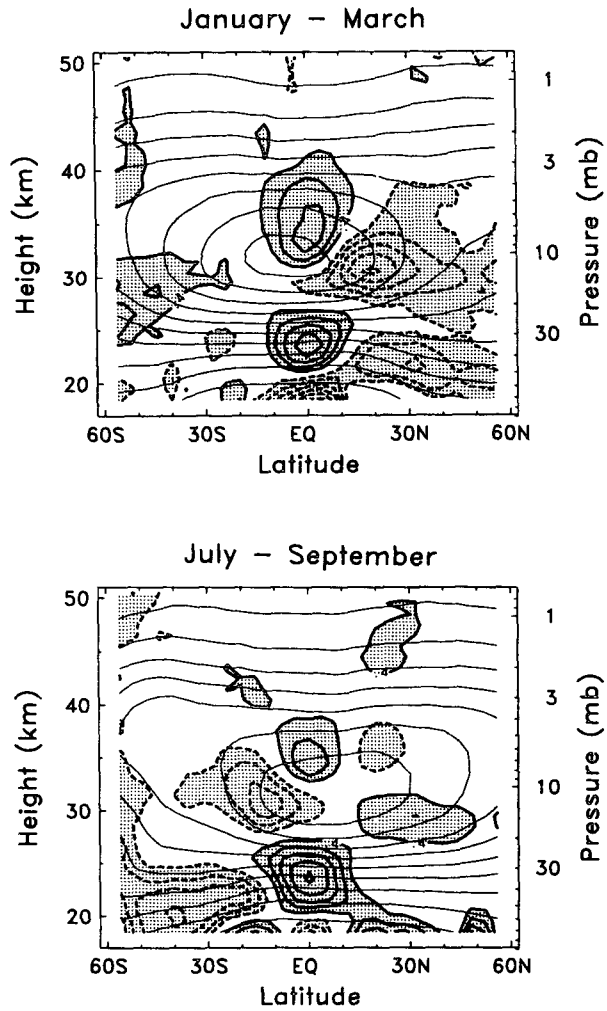


FIG. 10. Heavy solid and dashed lines with shading show seasonal variation of the regression coefficient $\alpha$ [Eq. (1)] for NH (top) and SH (bottom) winter–spring. Contours represent local percent variation, with arbitrary units. Light lines denote background zonal mean ozone for the corresponding time periods.

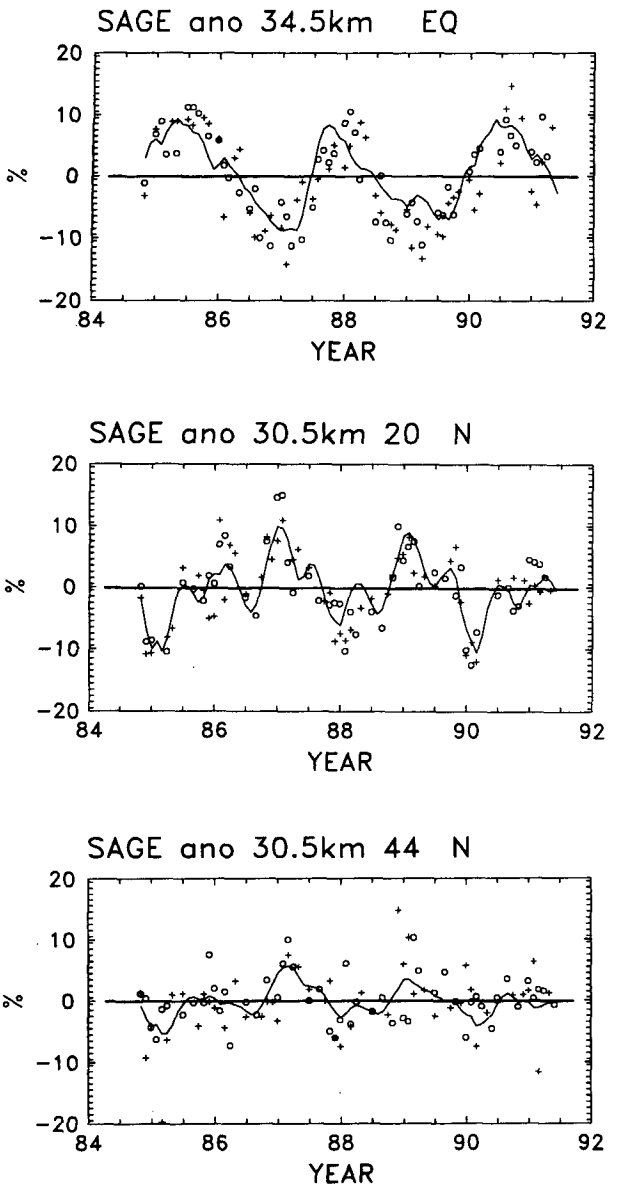


FIG. 11. Time series of interannual ozone anomalies for the same time series shown in Fig. 3. Smooth curves denote the QBO regression fit of these data using Eq. (1).

### c. *Variations in $NO_2$ and ozone chemistry*

Zawodny and McCormick (1991) proposed that $NO_2$ variations may be important for the observed middle-stratospheric ozone QBO signal, and Chipperfield et al. (1994) have modeled the associated chemical variations. We extend our analyses by extracting the QBO signal in SAGE II $NO_2$ data in an analogous manner to that used above, in order to study details of the global ozone $-NO_2$ coupling.

Figure 15 shows the two dominant SVD structures associated with QBO variations in $NO_2$, superimposed on the background (annual mean) $NO_2$ structure. QBO variations are observed in the Tropics and low–mid-latitudes of the middle stratosphere, with structure similar to the middle-stratosphere ozone patterns seen in Fig. 6. The subtropical maxima in SVD1 and equatorially centered pattern of SVD2 suggest that these regions are approximately in quadrature. The $NO_2$ anomalies in Fig. 15 occur in the region of strong background vertical gradients, although because $NO_2$ itself is not a conservative tracer, it is not clear from this diagnostic alone how to partition transport versus chemical effects.

Figure 16 shows the QBO $NO_2$ variations at the equator, derived from a regression analysis in an identical manner to the ozone data above. The QBO anom-

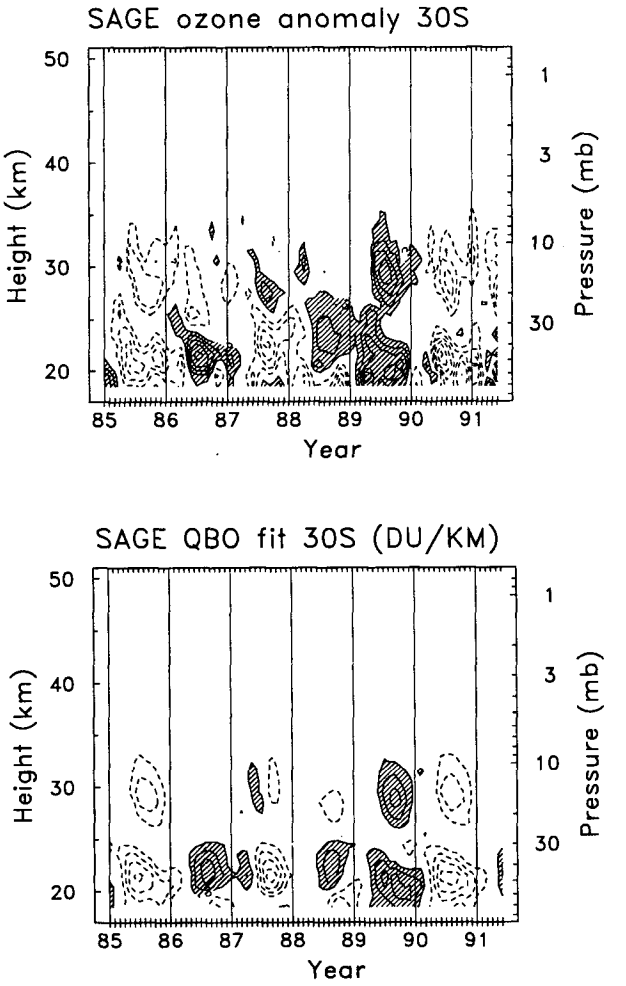


FIG. 12. Altitude–time sections of interannual ozone density anomalies at 30°S. Top panel shows full anomalies, and bottom panel shows the statistical QBO fit. Contours interval is 0.3 DU/km, with zero contours omitted.

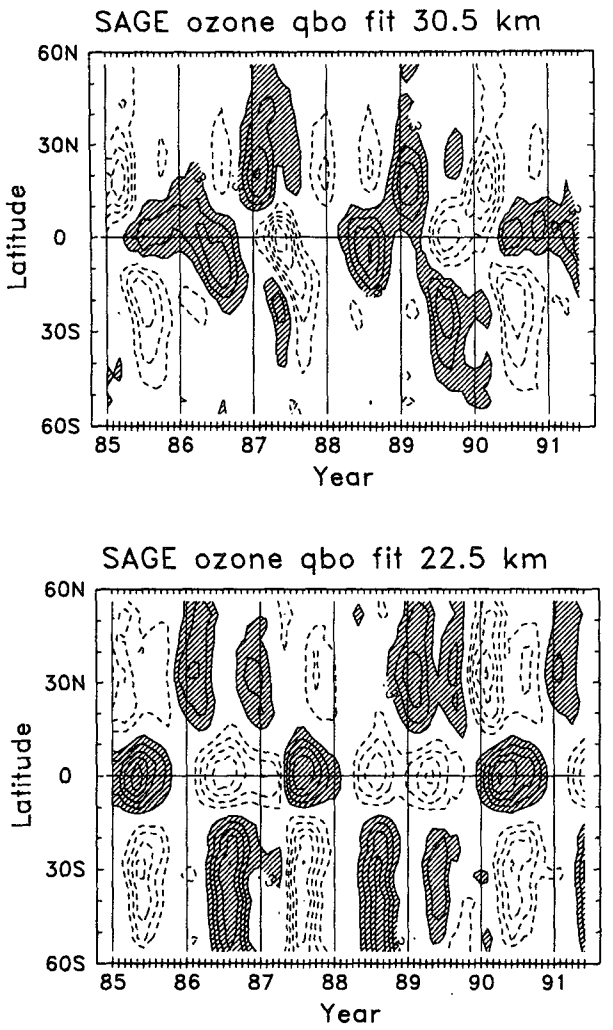


FIG. 13. Latitude–time sections of QBO-fit ozone density anomalies at 30.5 (top) and 22.5 km (bottom). Contour interval in both panels is 0.3 DU/km, with zero contours omitted.

alies in Fig. 16 show maxima over ~27–35 km, with slight downward propagation in time. Figure 17 shows similar plots for the latitude–time variations of $NO_2$ at 30.5 km, for both the full anomalies and the QBO-fit component. Large $NO_2$ anomalies are observed in both Tropics and midlatitudes, with values in Fig. 17 representing ± 30% variations with respect to the long-term mean. Comparison between the full and QBO-fit anomalies shows that the QBO explains a large fraction of the interannual $NO_2$ variability in the midstratosphere for this 6.5-yr record, in particular for variations away from the equator.

Comparison of the QBO $NO_2$ anomalies in Figs. 16–17 with the middle-stratosphere ozone anomalies in Figs. 4 and 13 shows strong anticorrelation, with nearly all details echoed in both datasets. Figure 18 shows a contour plot of the correlation between QBO fit ozone and $NO_2$ anomalies, calculated at each latitude and altitude. Given approximately 5 degrees of freedom for the 2.5 cycles of QBO data here (two independent pieces of information per cycle), correlations above approximately 0.75 are statistically significant at the 95% level. (The QBO regression analysis is effectively a very narrow bandpass filter; such filtering necessitates high correlation significance levels.) Figure 18 shows strong negative correlations over approximately 28–35 km for most of the region 50°N–40°S, with the correlations extending to slightly higher and lower altitudes outside of the Tropics. Small regions of positive correlation are seen near 25 km (discussed further be-

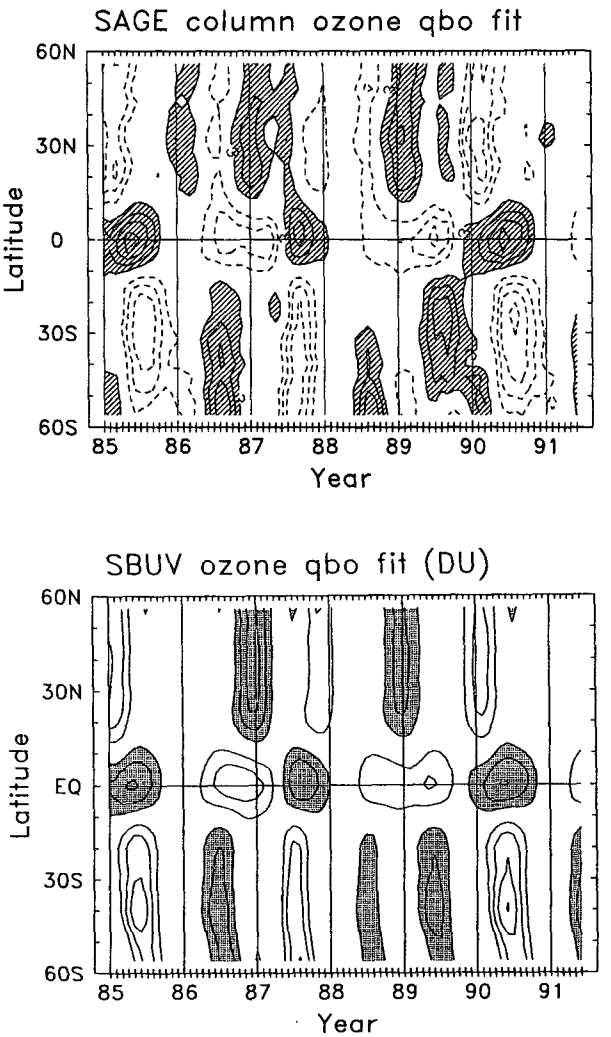


FIG. 14. Latitude–time sections of QBO column ozone anomalies derived from SAGE II data (top) and combined SBUV + SBUV/2 data (bottom). The SAGE II column anomalies are calculated by vertically integrating the ozone density data, as shown in Figs. 12–13. Contour interval is 3 DU, and zero contours are omitted.

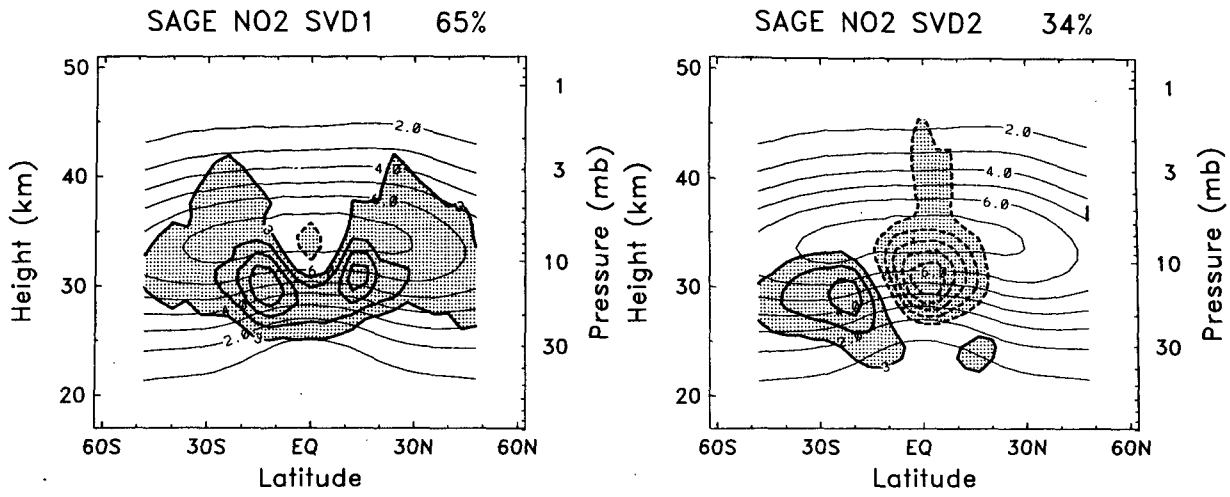


FIG. 15. Heavy solid and dashed lines with shading show spatial structure of QBO SVD1 (left) and SVD2 (right) for nitrogen dioxide. Contours show local mixing ratio variations with arbitrary units. Light lines show background annual average zonal mean $NO_2$ structure.

low). Positive ozone–$NO_2$ correlations are also seen in the tropical upper stratosphere (38–45 km), and this likely reflects that the sunset conversion of NO to $NO_2$ in this region depends directly on the amount of ozone.

Examples of the equatorial ozone–$NO_2$ correlations in the 26–34-km range are shown in the scatter plots in Fig. 19 (using data over ± 10° latitude). Data at 26.5 km show a positive correlation, together with some scatter related to phase lag of the $NO_2$ with respect to ozone (denoted by clockwise time progression of the anomaly points in Fig. 19). At lower altitudes (22–25 km, not shown here) the phase lag is near 90 (ozone leading $NO_2$), which is why the contemporaneous correlation is low (Fig. 18). The positive ozone–$NO_2$ correlations near 26.5 km (and at somewhat lower altitudes away from the equator; see Fig. 18) may be suggestive of a change over between nitrogen ($NO_x$)-related ozone losses above and hydrogen ($HO_x$)-dominated losses below (e.g., Garcia and Solomon 1994, their Fig. 8). Note that $HO_x$ and $NO_x$ are inversely related by reactions such as

$$OH + NO_2 \rightarrow HNO_3.$$

Thus decreased $NO_x$ will lead to increased $HO_x$, and enhanced ozone losses (yielding positive $NO_x$–ozone correlations).

The strong negative ozone–$NO_2$ correlations for the altitude region 28–35 km clearly points to $NO_x$-dominated ozone loss processes. With increased altitude in the Tropics, two features occur in the scatter plots in Fig. 19: 1) the ozone–$NO_2$ slope increases (i.e., ozone is more sensitive to $NO_2$) and 2) the scatterdiagram departs from linearity, with a phase lag introduced above 32 km ($NO_2$-leading ozone). The increased ozone sensitivity between 28.5 and 34.5 km implied in these SAGE II data is in good agreement with the model calculations of Chipperfield et al. (1994), shown in their Fig. 4, which they explain as due to an increase in background $NO_2$. The introduction of a phase lag above 32 km is likely an indication of ozone response to QBO temperature variations above this altitude.

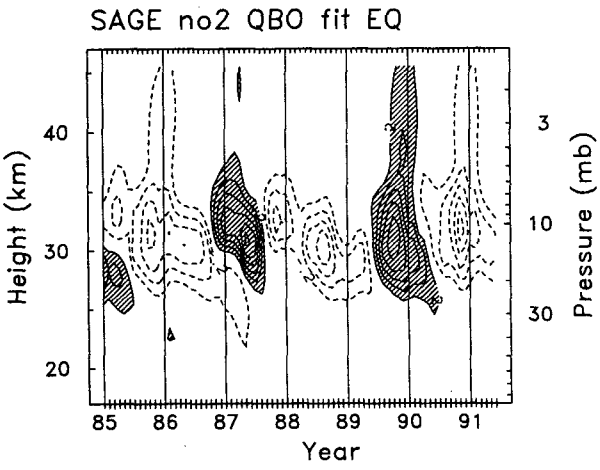


FIG. 16. Altitude–time section of QBO-fit $NO_2$ mixing ratio anomalies over the equator. Contours are 0.2 ppbv, and zero contours are omitted.

## 4. Summary and discussion

Singular-value decomposition provides a powerful tool to determine the space and time characteristics of coupled variations between two fields of data. In the application here we have chosen one field to represent the equatorial QBO and the other the "full" interan-

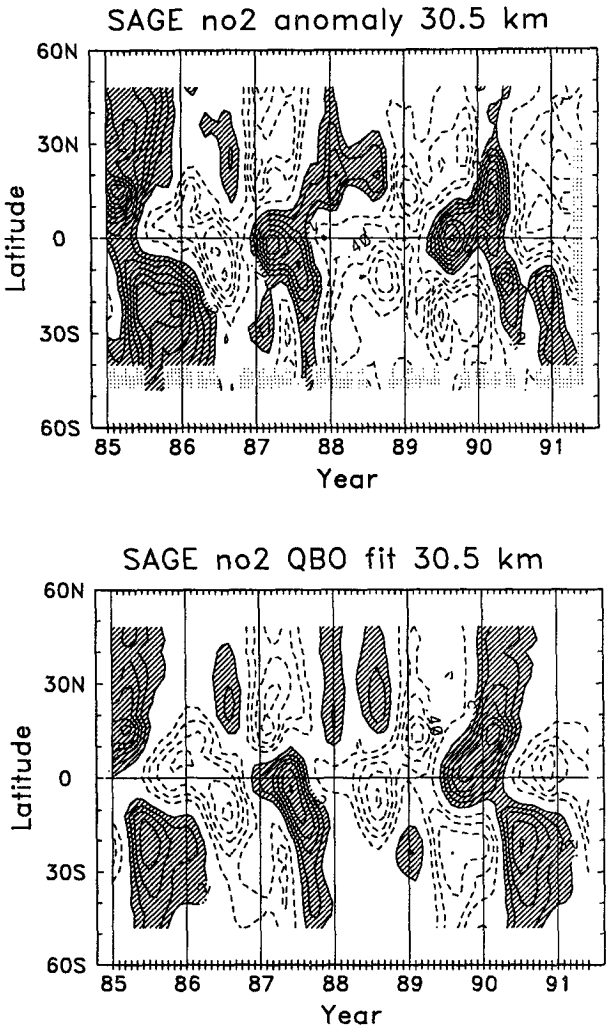


FIG. 17. Latitude–time sections of interannual $NO_2$ mixing ratio anomalies at 30.5 km. Top panel shows "full" anomalies, and lower panel shows the QBO-fit component. Contour interval in both panels is 0.2 ppmv, with zero contours omitted.

nual variations of SAGE II constituent data; the output of the SVD analysis is then by construction the global constituent QBO structure. This technique provides a novel view of the global ozone QBO, showing clear coupling of the equatorial and midlatitude components (Fig. 6), and quasi-regular global amplitude and phase propagation (Fig. 8). The amplitude of the ozone QBO appears related to the zonal wind QBO, at least for the short 2.5 cycle record here (Fig. 9).

Because seasonal variation is not explicitly included in the SVD analyses, we use a seasonally varying regression analysis to isolate local QBO variations. We use two independent QBO reference time series based on optimal linear combinations of the zonal winds over 70–10 mb, as determined by the SVD analyses. The overall results of the coupled SVD regression analyses act as an accurate digital filter to isolate QBO variations in the Tropics and midlatitudes. Accurate statistical isolation of the ozone QBO signal is not particularly important in the Tropics, where the QBO completely dominates other signals (see Fig. 4); conversely the QBO component in midlatitudes is similarly sized to other interannual variations (see Fig. 1), so that accurate separation is crucial for understanding both the QBO and "other" variability.

The prior analyses of SAGE II data by Zawodny and McCormick (1991) and Hasebe (1994) have focused on the tropical ozone QBO, documenting the clear double-peaked structure in altitude (shown in Fig. 4). The analyses here show a similar double-peaked ozone QBO structure in midlatitudes, with the two maxima in phase (versus near quadrature over the equator) and seasonally synchronized (with maxima in the respective winter–spring hemispheres). The lower-stratospheric maxima span a broad latitude range (~15°–60°, see Figs. 10 and 13) and occur in the region of strongest background vertical gradient (Figs. 6 and 10). This latter structure suggests that these anomalies are related to mean vertical circulation changes.

The middle-stratospheric ozone QBO anomalies peak in the subtropics (~10°–40°) and are coherent in space and time (and out of phase) with QBO variations in $NO_2$ (cf. Figs. 13a and 17b). This association points to reactive nitrogen chemical effects as the cause of the middle-stratospheric ozone anomalies, as confirmed by the modeling study of Chipperfield et al. (1994). An observed ozone–$NO_2$ phase lag above 32 km (Fig. 19) suggests ozone temperature sensitivity may also be important above this altitude. QBO variations in $NO_2$ occur in the region of strong background vertical gradi-

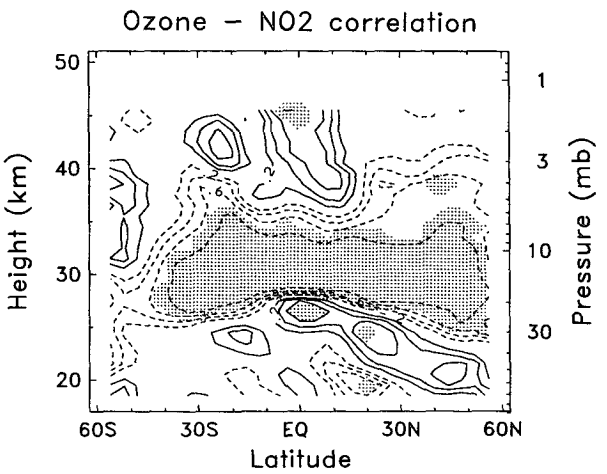


FIG. 18. Contour plot of the correlation between QBO-fit ozone and $NO_2$ anomalies. Contour interval is 0.2, with zero contours omitted. Shaded values (above 0.75) are statistically significant at the 95% level.

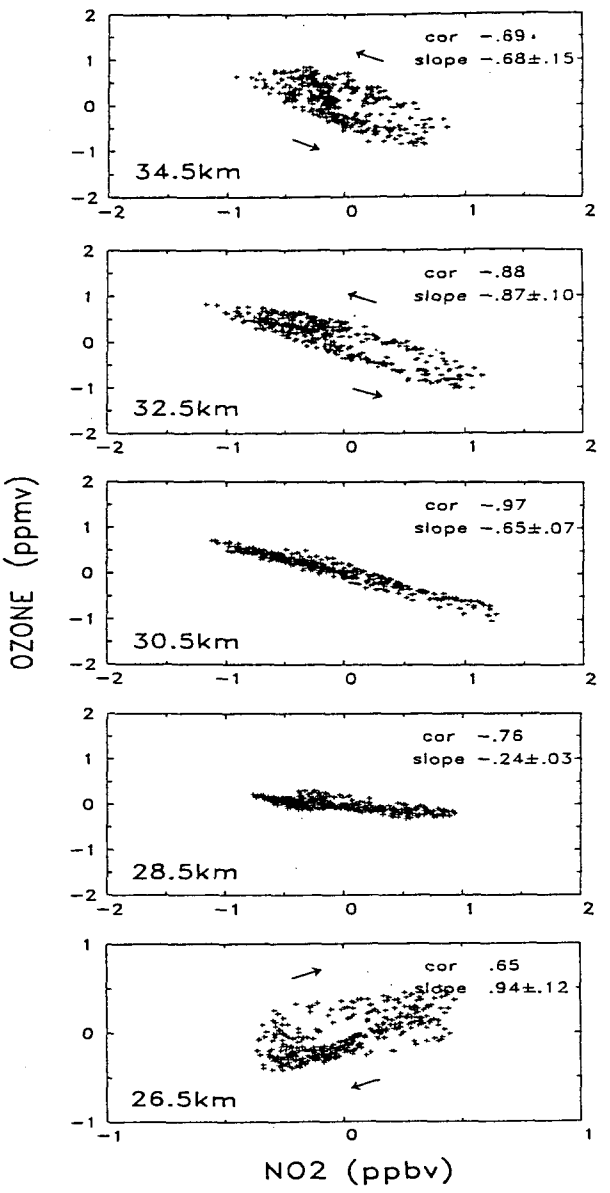


FIG. 19. Scatter diagrams of QBO variations in ozone and $NO_2$ near the equator at 26.5 (bottom) to 34.5 km (top). The correlation and slope at each location is indicated. Note that the scales in the lower panel are expanded by a factor of 2. Arrows denote time progression of the anomalies: clockwise rotation implies ozone leading $NO_2$ in time.

ents (Fig. 15), suggesting association with vertical circulation anomalies (although $NO_2$ is not a tracer and detailed study of total reactive nitrogen would be necessary for quantitative analyses). The observation that the upper-level $NO_2$ and lower-level ozone patterns are both seasonally synchronized (occurring only in the winter hemisphere) is clear evidence of large-scale winter circulation anomalies, such as those in the conceptual model of Tung and Yang (1994b) (due to QBO modulation of planetary waves and residual mean circulation).

Sophisticated attempts at modeling the extratropical ozone QBO have been reported in several recent studies (Gray and Pyle 1989; Holton 1989; Gray and Dunkerton 1992; Gray and Ruth 1993; Tung and Yang 1994b; Hess and O'Sullivan 1995). The SAGE II data show that ozone anomalies in the middle stratosphere are an important component of the midlatitude QBO, contributing one-third to one-half of the column anomalies over 10°–40°. Neglect of this important contribution will confuse quantitative comparisons between modeled and observed QBO column ozone in midlatitudes.

*Acknowledgments.* We thank Chip Trepte for supplying the SAGE II profile data and Barbara Naujokat for updated QBO winds. We also acknowledge Mike Wallace and Grant Branstator for discussions on statistical analyses, and Ian Plumb for chemistry expertise. This work was partially supported under NASA Grants W-16215 and W-18181 and NOAA Grant NAAZ0000300149.

## REFERENCES

Bhartia, P. K., J. Herman, R. D. McPeters, and O. Torres, 1993: Effects of Mt. Pinatubo aerosols on total ozone measurements from backscatter ultraviolet (BUV) experiments. *J. Geophys. Res.*, **98,** 18 547–18 554.

Bowman, K. P., 1989: Global patterns of the quasi-biennial oscillation in total ozone. *J. Atmos. Sci.*, **46,** 3382–3343.

Bretherton, C. S., C. Smith, and J. M. Wallace, 1992: An intercomparison of methods for finding coupled patterns in climate data. *J. Climate,* **5,** 541–560.

Chandra, S., and R. S. Stolarski, 1991: Recent trends in stratospheric total ozone: Implications of dynamical and El Chichón perturbations. *Geophys. Res. Lett.,* **18,** 2277–2280.

Chipperfield, M. P., and L. J. Gray, 1992: Two-dimensional model studies of the interannual variability of trace gases in the middle atmosphere. *J. Geophys. Res.,* **97,** 5963–5980.

——, ——, J. S. Kinnersley, and J. Zawodny, 1994: A two-dimensional model study of the QBO signal in SAGE II $NO_2$ and $O_3$. *Geophys. Res. Lett.,* **21,** 589–592.

Garcia, R. R., and S. Solomon, 1987: A possible relationship between interannual variability in Antarctic ozone and the quasi-biennial oscillation. *Geophys. Res. Lett.,* **14,** 848–851.

——, and ——, 1994: A new numerical model of the middle atmosphere, 2, Ozone and related species. *J. Geophys. Res.,* **99,** 12 937–12 952.

Gray, L. J., and J. A. Pyle, 1989: A two-dimensional model of the quasi-biennial oscillation in ozone. *J. Atmos. Sci.,* **46,** 203–220.

——, and M. P. Chipperfield, 1990: On the interannual variability of trace gasses in the middle atmosphere. *Geophys. Res. Lett.,* **17,** 933–936.

——, and T. J. Dunkerton, 1990: The role of the seasonal cycle in the quasi-biennial oscillation of ozone. *J. Atmos. Sci.,* **47,** 2429–2451.

——, and S. Ruth, 1993: The modeled latitudinal distribution of the ozone quasi-biennial oscillation using observed equatorial winds. *J. Atmos. Sci.,* **50,** 1033–1046.

Hamilton, K., 1989: Interhemispheric asymmetry and annual synchronization of the ozone quasi-biennial oscillation. *J. Atmos. Sci.,* **46,** 1019–1025.

Hasebe, F., 1983: Interannual variations of global ozone revealed from *Nimbus* 4 BUV and ground based observations. *J. Geophys. Res.*, **88,** 6819–6834.

——, 1994: Quasi-biennial oscillations of ozone and diabatic circulation in the equatorial stratosphere. *J. Atmos. Sci.,* **51,** 729–745.

Hess, P. G., and D. O'Sullivan, 1995: A three-dimensional modeling study of the extratropical quasi-biennial oscillation in ozone. *J. Atmos. Sci.,* **52,** 1539–1554.

Hollandsworth, S. M., R. D. McPeters, L. E. Flynn, W. Planet, A. J. Miller, and S. Chandra, 1995a: Ozone trends deduced from combined *Nimbus* 7 SBUV and NOAA SBUV/2 data. *Geophys. Res. Lett.,* **22,** 905–908.

——, K. P. Bowman, and R. D. McPeters, 1995b: Observational study of the quasi-biennial oscillation in ozone. *J. Geophys. Res.,* **100,** 7347–7361.

Holton, J. R., 1989: Influence of the annual cycle in meridional transport on the quasi-biennial oscillation in total ozone. *J. Atmos. Sci.,* **46,** 1434–1439.

Lait, L. R., M. R. Schoeberl, and P. A. Newman, 1989: Quasi-biennial modulation of the Antarctic ozone depletion. *J. Geophys. Res.,* **94,** 11 559–11 571.

McCormick, M. P., J. M. Zawodny, R. E. Viega, J. C. Larson, and P. H. Wang, 1989: An overview of SAGE I and II ozone measurements. *Planet. Space Sci.,* **37,** 1567–1586.

Oltmans, S. J., and J. London, 1982: The quasi-biennial oscillation in atmospheric ozone. *J. Geophys. Res.,* **87,** 8981–8989.

Perliski, L. M., and J. London, 1989: Satellite observed long-term averaged seasonal and spatial ozone variations in the stratosphere. *Planet. Space Sci.,* **37,** 1509–1525.

Randel, W. J., and J. B. Cobb, 1994: Coherent variations of monthly mean column ozone and lower stratospheric temperature. *J. Geophys. Res.,* **99,** 5433–5447.

——, and F. Wu, 1995: Climatology of stratospheric ozone based on SBUV and SBUV/2 data: 1978–1994. Tech. Note NCAR/TN-412+STR, National Center for Atmospheric Research, Boulder, CO, 137 pp.

Trepte, C. R., and M. H. Hitchman, 1992: Tropical stratospheric circulation deduced from satellite aerosol data. *Nature,* **355,** 626–628.

Tung, K. K., and H. Yang, 1994a: Global QBO in circulation and ozone. Part I: Reexamination of observational evidence. *J. Atmos. Sci.,* **51,** 2699–2707.

——, and ——, 1994b: Global QBO in circulation and ozone. Part II: A simple mechanistic model. *J. Atmos. Sci.,* **51,** 2708–2721.

Wallace, J. M., C. Smith, and C. S. Bretherton, 1992: Singular value decomposition of wintertime sea surface temperature and 500-mb height anomalies. *J. Climate,* **5,** 561–576.

——, R. L. Panetta, and J. Estberg, 1993: Representation of the equatorial quasi-biennial oscillation in EOF phase space. *J. Atmos. Sci.,* **50,** 1751–1762.

Yang, H., and K. K. Tung, 1994: Statistical significance and pattern of extratropical QBO in column ozone. *Geophys. Res. Lett.,* **21,** 2235–2238.

Zawodny, J. M., and M. P. McCormick, 1991: Stratospheric Aerosol and Gas Experiment II measurements of the quasi-biennial oscillation in ozone and nitrogen dioxide. *J. Geophys. Res.,* **96,** 9371–9377.